THE ROLE OF QUENCHING TIME IN THE EVOLUTION OF THE MASS–SIZE RELATION OF PASSIVE GALAXIES FROM THE WISP SURVEY[*]

A. Zanella[1,2,3], C. Scarlata[1], E. M. Corsini[2,4], A. G. Bedregal[5], E. Dalla Bontà[2,4], H. Atek[6], A. J. Bunker[7,8], J . Colbert[9], Y. S. Dai[10], A. Henry[11,16], M. Malkan[12], C. Martin[13], M. Rafelski[11,16], M. J. Rutkowski[1], B. Siana[14], and H. Teplitz[15]

[1] Minnesota Institute for Astrophysics, University of Minnesota, Minneapolis MN 55455, USA; anita.zanella@cea.fr
[2] Dipartimento di Fisica e Astronomia "G. Galilei," Università di Padova, vicolo dell'Osservatorio 3, I-35122 Padova, Italy
[3] Laboratoire AIM, CEA/DSM-CNRS-Université Paris Diderot, Irfu/Service d'Astrophysique, CEA Saclay, Orme des Merisiers, F-91191 Gif-sur-Yvette Cedex, France
[4] INAF—Osservatorio Astronomico di Padova, vicolo dell'Osservatorio 5, I-35122, Padova, Italy
[5] Department of Physics and Astronomy, Tufts University, Medford, MA 02155, USA
[6] Spitzer Science Center, Caltech, Pasadena, CA 91125, USA
[7] Department of Physics, University of Oxford, Denys Wilkinson Building, Keble Road, Oxford, OX13RH, UK
[8] Affiliate Member, Kavli Institute for the Physics and Mathematics of the universe, 5-1-5 Kashiwanoha, Kashiwa, 277-8583, Japan
[9] Harvard-Smithsonian Center for Astrophysics, 60 Garden Street, Cambridge, MA 02138, USA
[10] Infrared Processing and Analysis Center, 770 South Wilson Avenue, Pasadena, CA 91125, USA
[11] Goddard Space Flight Center, Code 665, Greenbelt, MD 20771, USA
[12] Department of Physics & Astronomy, University of California Los Angeles, Los Angeles, CA 90095, USA
[13] Department of Physics, University of California, Santa Barbara, CA, 93106, USA; cmartin@physics.ucsb.edu
[14] Department of Physics & Astronomy, University of California Riverside, Riverside, CA 92521, USA
[15] Infrared Processing and Analysis Center, Caltech, Pasadena, CA 91125, USA

ABSTRACT

We analyze how passive galaxies at $z \sim 1.5$ populate the mass–size plane as a function of their stellar age, to understand if the observed size growth with time can be explained with the appearance of larger quenched galaxies at lower redshift. We use a sample of 32 passive galaxies extracted from the Wide Field Camera 3 Infrared Spectroscopic Parallel (WISP) survey with spectroscopic redshift $1.3 \lesssim z \lesssim 2.05$, specific star formation rates lower than $0.01\,\mathrm{Gyr}^{-1}$, and stellar masses above $4.5 \times 10^{10}\,M_\odot$. All galaxies have spectrally determined stellar ages from fitting of their rest-frame optical spectra and photometry with stellar population models. When dividing our sample into young (age $\leqslant$2.1 Gyr) and old (age >2.1 Gyr) galaxies we do not find a significant trend in the distributions of the difference between the observed radius and that predicted by the mass–size relation. This result indicates that the relation between the galaxy age and its distance from the mass–size relation, if it exists, is rather shallow, with a slope $\alpha \gtrsim -0.6$. At face value, this finding suggests that multiple dry and/or wet minor mergers, rather than the appearance of newly quenched galaxies, are mainly responsible for the observed time evolution of the mass–size relation in passive galaxies.

Key words: galaxies: evolution – galaxies: fundamental parameters – galaxies: high-redshift – galaxies: structure

1. INTRODUCTION

In recent years many efforts have been devoted to observing early-type galaxies (ETGs) at high redshift to understand how these objects assembled, evolved, and became quenched. The discovery of a widespread population of passively evolving ETGs at redshift $z > 1.5$ showed that the star formation quenching in massive galaxies was already under way by $z \sim 2$ (e.g., Mancini et al. 2010). A large fraction of these high redshift passive galaxies show effective radii between a factor of 2 and 5 smaller than local counterparts of comparable stellar masses (e.g., Daddi et al. 2005). This result has been confirmed by several studies (e.g., Trujillo et al. 2007; Cimatti et al. 2008; Cassata et al. 2010; Carollo et al. 2013; van der Wel et al. 2014), and found to be robust with respect to bias against low surface brightness at high redshifts (e.g., Valentinuzzi et al. 2010). In the local universe, ETGs with similar stellar densities appear to be quite rare (Trujillo et al. 2009; Poggianti et al. 2012), although it has been suggested that they could

have survived as the cores of present-day massive spheroids (Hopkins et al. 2009; van Dokkum et al. 2014).

This discovery has ignited an important debate. The problem is not the existence of these compact ETGs: $z \sim 3$ submillimeter galaxies have comparable masses, sizes and number density, and have been identified as their possible precursors (e.g., Cimatti et al. 2008; Bedregal et al. 2013). The open issue is how these high-z compact galaxies can evolve to their present form, inflating their sizes up to a factor of 4, while at the same time following the tight correlations observed in the local universe (e.g., the fundamental plane).

Various mechanisms have been suggested to explain the growth of ETGs with time, although observations are still inconclusive as to which of them may be favorable. One of the most popular mechanisms invokes the accretion of multiple small satellites (e.g., Naab et al. 2009). These minor mergers leave the mass of the main galaxy relatively unchanged, while completely disrupting the satellites through strong tidal interactions. The accretion of stripped infalling stellar material is expected to increase the size of the merger remnant, without igniting intense star formation, particularly if the satellites do not contain large amounts of gas (e.g., Hopkins et al. 2009;

Oser et al. 2012). Some observational studies suggest that this mechanism may account for ∼50% of the apparent size evolution, at least at redshift $0 < z < 1$ (López-Sanjuan et al. 2012; Newman et al. 2012). Despite the implications of these observational results, there is a problem explaining the size evolution with multiple minor mergers. Nipoti et al. (2012) found that multiple minor mergers would introduce more scatter than observed in the low-redshift scaling relations that link the galaxy stellar mass, effective radius and velocity dispersion, unless the progenitors were already finely tuned to occupy a very tight region in the mass–radius plane. Such fine tuning is difficult to explain, and leaves open the question of *when* and *how* the mass–size relation is first created. Moreover, Hopkins et al. (2009) highlighted that in the merging scenario a non-negligible fraction of compact galaxies ($\lesssim 10\%$) should survive to $z \sim 0$, while observations by Trujillo et al. (2009) show that only 0.03% of local galaxies have stellar densities comparable to those of high redshift ETGs.

Adiabatic expansion through significant mass loss can also lead to size growth (Fan et al. 2010). A galaxy that loses mass as a result of supernova/AGN-driven winds will adjust its size in response to the shallower central potential (Newman et al. 2012). This mechanism would induce a sort of "puffing-up" of the galaxy arising from the loss of baryonic mass, with an effective size increase. However, the puffing-up only occurs when the system is highly active and young (in terms of its stellar population, Ragone-Figueroa & Granato 2011), and produces a fast expansion (a few dynamical times, $\sim 10^8$ years). Thus one would expect only a minority of objects to be passive and compact, at odds with observations.

The problem has also been explored from a different perspective (the so called "progenitor bias" scenario): instead of explaining the evolution of the mass–size relation with the growth of *individual* galaxies with time, it has been suggested that it is the *population* of ETGs that changes, with larger quenched galaxies appearing later (Valentinuzzi et al. 2010; Saracco et al. 2011; Cassata et al. 2013). This may be linked to the evolution of the average density in the universe due to Hubble expansion, with lower density halos collapsing later in time than denser ones (e.g., Saracco et al. 2011; Carollo et al. 2013). However, the relative importance of the two mechanisms (individual versus population growth) is still highly controversial (Bernardi et al. 2010; Cassata et al. 2011; Poggianti et al. 2013; van der Wel et al. 2014; Belli et al. 2015; Keating et al. 2015). If the redshift evolution of the mass–size relation is due to the appearance of newly quenched large galaxies, then one would expect that, at any given mass and time, the larger galaxies should on average be younger than the smaller ones. Here we test this prediction using a sample of $z \sim 1.5$ passive ETGs observed as part of the Wide Field Camera 3 (WFC3) Infrared Spectroscopic Parallel (WISP) survey (Atek et al. 2010).

Throughout the paper we assume a flat cosmology with $H_0 = 70 \, \mathrm{km \, s^{-1} \, Mpc^{-1}}$, $\Omega_M = 0.3$, and $\Omega_\Lambda = 0.7$. Photometric magnitudes are expressed in the AB system (Oke & Gunn 1983).

2. OBSERVATIONS AND DATA ANALYSIS

The sample presented in this work includes 34 passive galaxies identified in the WISP survey, a pure-parallel *Hubble Space Telescope* (*HST*) program to obtain near-infrared slitless spectra together with optical and infrared (IR) imaging of hundreds of independent fields in the sky. The data have been presented in detail in Atek et al. (2010). Briefly, we consider here the first 27 fields observed with both *HST* WFC3 grisms (G102, and G141; with resolving power $R = 210$ and 130, respectively), as well as with the WFC3-UVIS camera in the optical. The IR spectra cover the wavelength range between $0.85 \leqslant \lambda \leqslant 1.6 \, \mu m$, with approximately $0.1 \, \mu m$ overlap between the two grisms that allows us, together with the IR imaging, to check for proper photometric calibration and sky subtraction. The data were reduced and the spectra extracted with a combination of a custom pipeline described in Atek et al. (2010) and the aXe software (Kümmel et al. 2009). In addition, we implemented a new cleaning algorithm to properly account for contamination from overlapping spectra (see details in Bedregal et al. 2013). The imaging was obtained with the F475X and F600LP (apart from the two deepest fields that were observed with F606W and F814W instead), and with the F110W and F160W filters, respectively (see Bedregal et al. 2013).

Bedregal et al. (2013) studied the properties of a sample of $H < 23$ mag galaxies preselected on the basis of their *J–H* color. They measured spectroscopic redshifts and stellar population properties of the galaxies by simultaneously fitting the broadband photometric points and spectra. Here we present the size measurements for the subsample of passive galaxies selected to have a specific star formation rate sSFR $\lesssim 0.01 \, \mathrm{Gyr}^{-1}$, redshift $z > 1.3$ and $M_* > 4.5 \times 10^{10} \, M_\odot$. This is the minimum stellar mass measurable at $z \sim 1.5$ (the average redshift of the sample), for a maximally old stellar population model (SPM). These limits have been chosen to select a sample of massive and passive galaxies and their robustness is discussed in Bedregal et al. (2013). If we were to consider a more conservative sample selection based on the minimum stellar mass measurable at $z \sim 2$ (the highest redshift in our sample) $M_* > 7.9 \times 10^{10} \, M_\odot$, our results would not change substantially (see Section 4). We verified that the stellar mass function of our galaxy sample is consistent with the one determined by Muzzin et al. (2013), for quiescent galaxies, at the same redshift. All galaxies have accurate luminosity-weighted stellar ages derived fitting the grism spectra with SPMs. Using the same set of simulations performed by Bedregal et al. (2013) we find that for our sample, the stellar ages are recovered with an accuracy of 35%.

3. SIZE ANALYSIS

For the structural analysis of the light distribution of our sample galaxies we use the deeper J_{110} images. The sky background has been previously subtracted as discussed in Atek et al. (2010) and Colbert et al. (2013). We perform the measurements with two different fitting algorithms: the widely used GALFIT code (Peng et al. 2010) and the alternative GASP2D code (Méndez-Abreu et al. 2008). To be consistent with previous works in the field, we fit the galaxy light distribution with a single Sérsic law (Sérsic 1963).

Both codes require as input the instrumental Point-spread Function (PSF). Our data were taken in parallel to observations performed with the Cosmic Origin Spectrograph and Space Telescope Imaging Spectrograph, and no spatial dithering was done in between different exposures. Because of this, the final PSF is undersampled at the pixel size ($0.\!''13 \, \mathrm{pixel}^{-1}$) of the WFC3-IR camera. We provide both GALFIT and GASP2D with a PSF that we obtained as the median of 18 unsaturated

stars across the 27 analyzed fields. We used this median PSF to fit individual stars in each field, and found residuals of at most 20%, irrespective of the field. Before fitting the galaxies, we masked any foreground and background sources, as well as detector artifacts that can contaminate the surface brightness distribution. The main differences between the two codes is in the way the initial values for the parameters are determined. GALFIT does not provide a way to estimate them, while GASP2D internally determines their values by performing a fit on the one-dimensional surface brightness profile obtained using the IRAF task `ellipse` (see Méndez-Abreu et al. 2008 for details). We visually inspected all the residuals to check for the reliability of the fits and we find that for each sample galaxy they are lower than 20%.

The galaxy effective radii (r_e) measured with the two algorithms are consistent within the uncertainties. In the following analysis we use the sizes determined by GASP2D, but our conclusions would not change if we switch to GALFIT instead. For each galaxy we compute the circularized effective radius as $r_e^{circ} = r_e \sqrt{q}$, where q is the galaxy axial ratio.

We determine the uncertainties associated with the r_e measurements through Monte Carlo simulations. We created 1000 artificial galaxies with Sérsic parameters randomly chosen in the range of values observed for real galaxies (total magnitude $19 \leqslant m_{tot} \leqslant 24$, effective radius $0\rlap{.}''1 \leqslant r_e \leqslant 1\rlap{.}''5$, Sérsic index $0.5 \leqslant n \leqslant 12$, axial ratio $0.2 \leqslant q \leqslant 1$, position angle $0° \leqslant PA \leqslant 180°$). All the models were convolved with the PSF image and we added Poisson noise to reproduce the observations. The best-fit Sérsic parameters were then derived using both GALFIT and GASP2D.

For each parameter, we estimated the fractional uncertainty as

$$\epsilon = \frac{p_{out} - p_{in}}{p_{out}}, \qquad (1)$$

where p_{out} is the fitted parameter and p_{in} is the input value. We then computed the median and the 16th and 84th percentiles in bins of p_{out}, to estimate the systematics together with upper and lower uncertainties on the parameters. We excluded from the sample two galaxies with output effective radii smaller than 1 kpc since we believe that $r_e < 1$ kpc values are not reliable, and we therefore set 1 kpc as the minimum size we are able to resolve. With Monte Carlo simulations we also checked that galaxies with $r_e < 1$ kpc do not enter the sample with an overestimated size. This limit is higher than similar depth surveys performed with WFC3: it results from the lack of spatial dithering between exposures. With simulations we quantify the impact of this size limit on our results (Section 4). The uncertainty associated with the circularized radius is calculated as $\epsilon_{r_e}^{circ} = \epsilon_{r_e} \sqrt{q}$, because we find that the axial ratio uncertainty is negligible.

The Sérsic best-fit circularized half-light radius, Sérsic index, stellar mass, stellar age and redshift for each galaxy in the final sample are presented in Table 1. We notice that half of the galaxies in our sample have a Sérsic index $n < 2.5$, typically associated with disk-dominated galaxies, in agreement with, e.g., van der Wel et al. (2011) and Newman et al. (2014, hereafter N14).

Table 1
Circularized Effective Radius, Sérsic Index, Stellar Mass, Age, and Redshift of the Galaxies in the Final Sample

| Galaxy	r_e^{circ} (kpc)	n	$\log(M_\star/M_\odot)$	Age (Gyr)	z
(1)	(2)	(3)	(4)	(5)	(6)
Par66 ID135	1.33 ± 0.35	2.24	11.24	2.00	1.80
Par67 ID108	1.05 ± 0.33	1.07	10.71	1.02	1.35
Par67 ID140	1.75 ± 0.38	0.72	11.30	2.75	2.05
Par67 ID82	1.36 ± 0.26	2.29	11.08	4.00	1.35
Par73 ID152	2.71 ± 1.19	1.23	10.74	2.75	1.50
Par73 ID47	2.74 ± 0.17	4.03	11.16	0.90	1.45
Par73 ID57	1.67 ± 0.51	1.35	11.22	0.90	1.60
Par74 ID37	2.54 ± 0.82	1.72	11.44	2.50	1.60
Par76 ID26	2.32 ± 1.02	7.38	11.77	4.25	1.40
Par76 ID41	2.29 ± 0.84	0.74	11.26	4.75	1.35
Par76 ID60	2.96 ± 1.15	3.54	11.73	3.50	1.70
Par76 ID62	1.64 ± 0.59	17.53	11.50	3.50	1.70
Par76 ID77	1.23 ± 0.37	0.69	11.31	0.45	2.05
Par79 ID19	3.06 ± 0.70	7.92	11.55	2.20	1.35
Par79 ID86	1.53 ± 0.61	8.76	11.05	1.02	1.90
Par80 ID28	5.04 ± 0.56	4.15	11.43	4.00	1.40
Par80 ID35	1.73 ± 0.54	3.33	11.14	1.61	1.55
Par80 ID50	2.19 ± 0.51	1.10	11.17	3.00	1.40
Par80 ID93	4.13 ± 0.79	2.92	11.04	3.50	1.85
Par84 ID57	1.83 ± 0.57	2.09	11.43	4.00	1.45
Par87 ID118	3.14 ± 0.40	5.14	11.38	2.20	1.70
Par87 ID125	1.34 ± 0.53	7.29	10.66	0.40	1.85
Par87 ID54	1.28 ± 0.35	1.25	11.34	3.00	1.50
Par87 ID87	1.50 ± 0.53	6.05	11.12	2.00	1.65
Par87 ID95	2.73 ± 0.35	0.83	10.71	1.02	1.60
Par96 ID62	1.28 ± 0.35	2.47	10.91	1.02	1.75
Par115 ID83	2.04 ± 0.45	2.66	11.01	1.80	1.65
Par120 ID64	1.74 ± 0.54	3.43	11.23	1.61	1.50
Par120 ID84	4.01 ± 1.60	2.21	11.28	2.20	1.65
Par136 ID55	2.79 ± 1.22	2.11	10.68	0.90	1.65
Par136 ID77	3.55 ± 0.62	0.90	10.84	1.14	1.65
Par147 ID46	2.38 ± 1.04	2.52	11.02	0.64	1.46

Notes. Col. (1): galaxy name defined as in Bedregal et al. (2013). Col. (2): circularized effective radius with associated relative error. Col. (3): Sérsic index. Col. (4): logarithm of the stellar mass. Col. (5): age. Col. (6): redshift.

4. RESULTS AND DISCUSSION

We compare the stellar mass and size of our galaxies with those in the literature in the top panel of Figure 1. Before placing the literature data on the mass–size plane, we homogenized all the masses to Salpeter initial mass function (IMF, Salpeter 1955)[17] and corrected them for the systematics implied by the different ages of the adopted synthetic stellar population models (SPMs). We scaled all masses to the Bruzual & Charlot (2003) SPMs, adopting the Salimbeni et al. (2009) relations $\log(M_{M05}) \simeq \log(M_{CB07})$ and $\log(M_{M05,CB07}) = \log(M_{BC03}) - 0.2$ where BC03, M05, and CB07 indicate Bruzual & Charlot (2003), Maraston (2005), and Bruzual et al. (2007) SPMs, respectively.

We limit the comparison to only those works where the sample selection is based on the galaxy specific star formation rates and that span a similar redshift range to ours. The only exception is the Mancini et al. (2010) sample, where a

---

[17] The scaling factors between the Chabrier (2003), Kroupa (2001) and Salpeter (1955) IMFs that we adopted are: $\log(M_{Chabrier}) = \log(M_{Kroupa}) - 0.04$ (Cimatti et al. 2008) and $\log(M_{Chabrier}) = \log(M_{Salpeter}) - 0.25$ (Salimbeni et al. 2009).
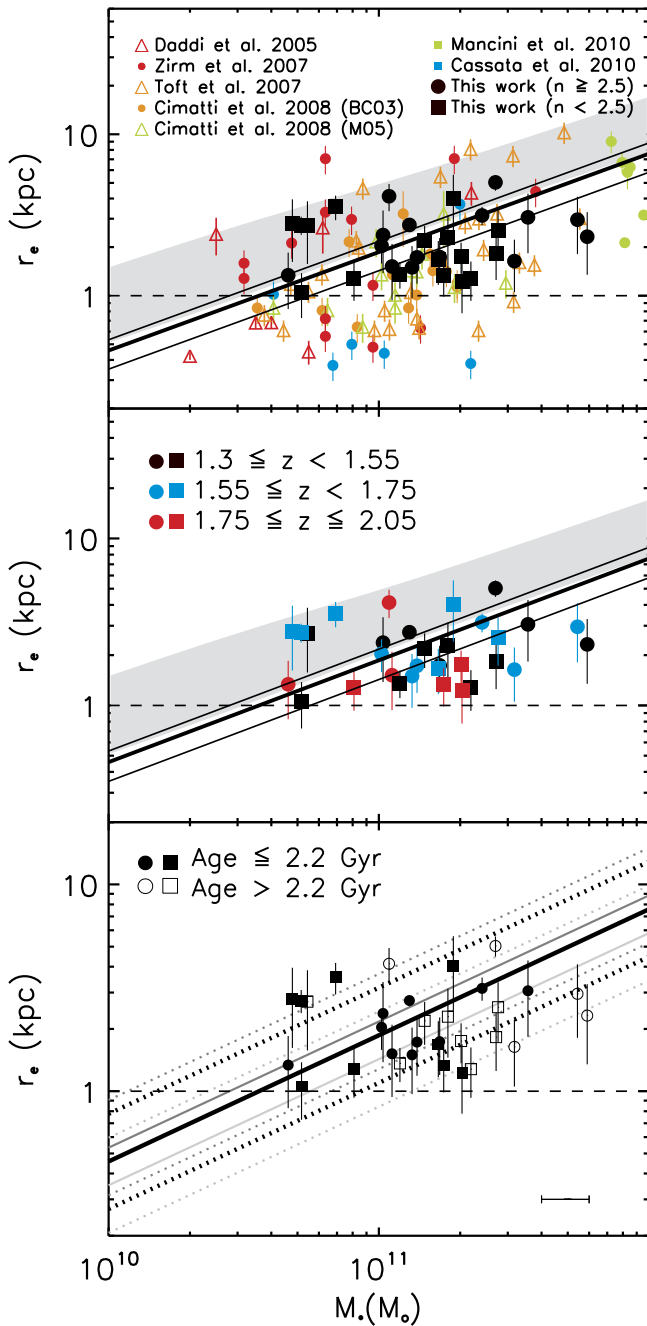
Figure 1. The mass–size relation measured with the WISP data at $z \sim 1.5$. We show circularized effective radius vs. stellar mass for the present sample (black symbols), with a distinction based on the Sérsic index (circles and squares), and compare the results drawn from the literature. Top: circularized effective radius vs. stellar mass. The local mass–size relation and its scatter (from Shen et al. 2003) are shown, for illustrative purposes, as a gray band. The solid thick line shows the best-fit mass–size relation from N14, computed at $z = 1.5$, while the thin lines were computed at the lowest (1.35) and highest (2.05) redshifts of our sample galaxies. All the galaxy radii shown here are circularized, except for those by Mancini et al. (2010). Middle: same as top panel, but showing our sample in three groups of redshift (black, blue, and red symbols). Again we separate galaxies with low and high Sérsic index (circles and squares). Bottom: same as the top panel, but showing our sample in two groups of stellar age (filled and empty symbols). In the bottom right corner we show the median uncertainty in stellar mass for our sample of galaxies (Bedregal et al. 2013). Our effective radii measurement limits are shown (dashed line).
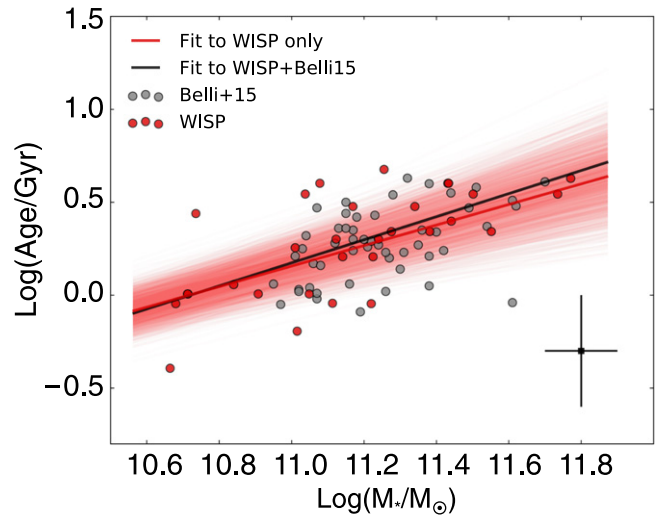

Figure 2. Stellar age and mass of quenched galaxies are strongly correlated. Stellar age as a function of stellar mass for the WISP galaxies (red points) and Belli et al. (2015) sample (gray points). Belli et al. (2015) stellar masses were converted to Salpeter IMF following Salimbeni et al. (2009). The best-fit lines to the WISP sample alone and to the combined WISP and Belli et al. (2015) samples are shown with red and black lines, respectively. The red band shows the uncertainty on the fit to the WISP data alone (the uncertainty on the fit to the combined sample is similar, and not shown for clarity).

morphological selection criterion (based on the Sérsic index) was also applied. Figure 1 shows that our measurements are consistent with the results found at similar redshifts by other works in different fields, once the size lower-limit (dashed horizontal line) is considered. The thick solid line shows the best-fit mass–size relation derived by N14 for field galaxies, computed at the median redshift of the sample. The thin lines were computed at the lowest and highest redshifts of our sample galaxies.

In the bottom panel of Figure 1 we reproduce the mass–size relation for our galaxies, dividing the sample into old (stellar age >2.1 Gyr) and young objects (age ⩽2.1 Gyr). The age separation was chosen to divide the galaxies in two similar size samples. Figure 1 shows how the most massive galaxies ($M_* > 2 \times 10^{11} M_\odot$) tend to be older than less massive ones, a trend compatible with other observational results indicating that more massive galaxies form the bulk of their stars earlier (e.g., Thomas et al. 2005; Kaviraj et al. 2013). We quantify this trend in Figure 2, where we show the stellar age versus the stellar mass, for the galaxies in our sample as well as for a sample of similarly selected objects identified by Belli et al. (2015). The correlation between the stellar population age and mass has a Spearman correlation coefficient of 0.66, which has a probability of 10^{-5} of resulting by chance. At any stellar mass, the stellar age (A_M) can be expressed as: $\log(A_M/\mathrm{Gyr}) = (0.55 \pm 0.09)\log M_{10.5} - (0.12 \pm 0.07)$, where $M_{10.5}$ is the stellar mass in units of $10^{10.5} M_\odot$.

To quantify whether a trend between the stellar age and the deviation from the $z \sim 1.5$ mass–size relation exists we compute for each galaxy the parameter $\Delta_{lr} = \log(R_{obs}/R_{M,z})$, i.e., the vertical difference between the observed galaxy size (R_{obs}) and the size expected from the galaxy's redshift and stellar mass ($R_{M,z}$), using the N14 mass–size relation. Values of $\Delta_{lr} > 0$ (<0) indicate that galaxies are above (below) the mass–size relation at the galaxy redshift. The distributions of Δ_{lr} for the old and young galaxies with $M_* > 4.5 \times 10^{10} M_\odot$
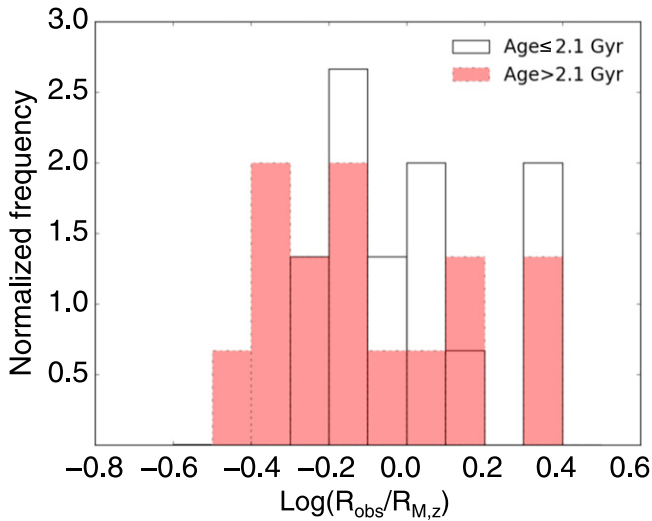
Figure 3. Distribution of Δ_{lr} for the WISP passive galaxies. Although the distributions of young and old galaxies have different median values, they are not statistically different. Pink and white lines represent old and young galaxies, respectively (see text for details).

are shown in Figure 3. The medians of the two distributions are $-0.02^{+0.36}_{-0.16}$ and $-0.13^{+0.31}_{-0.21}$, for the young and old samples, respectively (the upper and lower range show the 84th and 16th percentiles). The result of a two-sample Kolmogorov–Smirnoff (KS) test ($D_{KS} = 0.3$ and $p = 0.3$), however, indicates that we cannot exclude that the two samples are drawn from the same parent distribution and thus the observed age difference is not significant. More conservatively considering only galaxies with $M_* > 7.9 \times 10^{10} M_\odot$ we obtain consistent results (the medians of the young and old galaxy distributions of Δ_{lr} are $-0.10^{+0.09}_{-0.16}$ and $-0.18^{+0.17}_{-0.14}$, respectively).

The size measurement limit ($r_e > 1$ kpc), together with the observed dependency between the galaxy stellar age and mass, may introduce a bias, particularly at the smallest masses, where our galaxies tend to populate the mass–size plane above the best-fit relation derived at similar redshifts (N14). To test to what extent we can detect with our data a possible trend of the distance from the best-fit mass–size relation with age, we performed a simulation that accounts for both the size selection bias and the observed mass–age trend. We generated 1000 samples of 32 galaxies with masses and half-light radii distributed according to the field mass–size relation and its scatter, determined by N14 at $z \sim 1.5$. To each galaxy we assign an age (A) that depends on its stellar mass and the distance to the mass–size relation, such that $A = A_M + \alpha \Delta_{lr}$. We randomize the simulated ages and stellar masses according to the typical uncertainties of our observations. We then apply the WISP survey limits to the simulated galaxy samples (i.e., $M_* > 4.5 \times 10^{10} M_\odot$, and $r_e \geqslant 1$ kpc), and recompute the distributions of Δ_{lr} for the subsamples of old and young galaxies. For each of the 1000 samples we performed the same analysis described above, and compute the KS test between the distributions of Δ_{lr} for the young and old subsamples. For $\alpha = 0$ (i.e., no correlation), we find that only 10% of the simulated samples show detectable differences between the old and young galaxies, due to our size limit and the correlation between the age and stellar mass. We consider decreasing values of α in steps of 0.1, from zero to the α that produces distinguishable distributions. Our simulations show that for any

$\alpha < -0.64$ we would be able to recover the difference between old and young populations at the 95% confidence level in more than 85% of the simulated samples. Repeating the same simulations and applying a mass limit $M_* > 7.9 \times 10^{10} M_\odot$, we find $\alpha < -0.7$. Our data, therefore, suggest that the relation between the galaxy age and its distance from the mass–size relation, if it exists, must have $\alpha > -0.64$. Performing these simulations considering the galaxies formation redshift (z_f) instead of age, given the observed redshift and the current cosmology, we conclude that, if a relation $R \sim (1 + z_f)^\beta$ exists, then it must be $\beta > -0.67$, otherwise we would have detected the correlation with our current sample.

5. CONCLUSIONS

We studied the mass–size relation of a sample of 32 passive galaxies at $z \sim 1.5$ selected from the WISP survey to have sSFR < 0.01 Gyr^1 and $M_* > 4.5 \times 10^{10} M_\odot$. All galaxies have accurately determined stellar ages from fitting the galaxy rest-frame optical spectra with SPMs (Bedregal et al. 2013). We investigate whether younger galaxies have preferentially larger sizes than older ones with the same stellar mass. Such an observation would indicate that the mass–size relation evolves due to the appearance of newly quenched large objects in passive samples.

Dividing our sample into young and old galaxies we find no significant difference in the distributions of Δ_{lr}, suggesting that the appearance of newly quenched galaxies may not be the dominant mechanism for the evolution of the mass–size relation. Our simulations also indicate that, if a relation exists between the galaxy age and the distance to the mass–size relation, it has a slope $\alpha > -0.64$, otherwise we would have detected it. It translates into a slope of the galaxies size-formation redshift relation $\beta > -0.67$, given the current cosmology. If we consider in our analysis more conservatively only galaxies with $M_* > 7.9 \times 10^{10} M_\odot$ we obtain consistent results.

Our results suggest that the evolution of the mass–size relation of quiescent galaxies is mainly due to the physical growth of individual sources. Recently, Belli et al. (2015) have found that progenitor bias can explain half of the size growth of compact ETGs and that the remaining observed size evolution arises from a genuine growth of individual galaxies. The discrepancy is likely due to the fact that they include in the sample "green valley" sources, with sSFR <0.1 Gyr^{-1}, while we limit the analysis to those galaxies with sSFR <0.01 Gyr^{-1}. In fact, it is exactly these sources with higher sSFR that drive the correlation between the age and the size evolution (see Figure 9 in Belli et al. 2015). Our finding is in contradiction with works implying a slope of $\beta \sim -1$ for the size-formation redshift relation and suggesting that galaxies sizes scale as the density of the universe at the time when they formed (e.g., Saracco et al. 2011; Carollo et al. 2013; Cassata et al. 2013). Our results are instead in agreement with the ones by Trujillo et al. (2011) and Whitaker et al. (2012), which do not see any age segregation depending on the galaxy size. Sonnenfeld et al. (2014) suggest that the observed size growth cannot be explained with models invoking only dry merger, because they would result in a strong flattening of the mass density profile with time. This flattening is not observed in the samples of strong lenses for which the total mass–density profile could be constrained (Sonnenfeld et al. 2014). The size growth could

instead be due to a combination of dry and wet minor mergers: the outer regions of massive ETGs could grow via the accretion of stars and dark matter, while a small amount of nuclear star formation could keep the mass density profile constant with time (e.g., Rutkowski et al. 2014).

REFERENCES

Atek, H., Malkan, M., McCarthy, P., et al. 2010, ApJ, 723, 104
Bedregal, A. G., Scarlata, C., Henry, A. L., et al. 2013, ApJ, 778, 126
Belli, S., Newman, A. B., & Ellis, R. S. 2015, ApJ, 799, 206
Bernardi, M., Shankar, F., Hyde, J. B., et al. 2010, MNRAS, 404, 2087
Bruzual, G. 2007, arXiv:astro-ph/0703052
Bruzual, G., & Charlot, S. 2003, MNRAS, 344, 1000
Carollo, C. M., Bschorr, T. J., Renzini, A., et al. 2013, ApJ, 773, 112
Cassata, P., Giavalisco, M., Guo, Y., et al. 2010, ApJL, 714, L79
Cassata, P., Giavalisco, M., Guo, Y., et al. 2011, ApJ, 743, 96
Cassata, P., Giavalisco, M., Williams, C. C., et al. 2013, ApJ, 775, 106
Chabrier, G. 2003, PASP, 115, 763
Cimatti, A., Cassata, P., Pozzetti, L., et al. 2008, A&A, 482, 21
Colbert, J. W., Teplitz, H., Atek, H., et al. 2013, ApJ, 779, 34
Daddi, E., Renzini, A., Pirzkal, N., et al. 2005, ApJ, 626, 680
Fan, L., Lapi, A., Bressan, A., et al. 2010, ApJ, 718, 1460
Hopkins, P. F., Bundy, K., Murray, N., et al. 2009, MNRAS, 398, 898
Kaviraj, S., Cohen, S., Ellis, R. S., et al. 2013, MNRAS, 428, 925
Keating, S. K., Abraham, R. G., Schiavon, R., et al. 2015, ApJ, 798, 26
Kroupa, P. 2001, MNRAS, 322, 231
Kümmel, M., Walsh, J. R., Pirzkal, N., Kuntschner, H., & Pasquali, A. 2009, PASP, 121, 59
López-Sanjuan, C., Le Fèvre, O., Ilbert, O., et al. 2012, A&A, 548, A7
Mancini, C., Daddi, E., Renzini, A., et al. 2010, MNRAS, 401, 933
Maraston, C. 2005, MNRAS, 362, 799
Méndez-Abreu, J., Aguerri, J. A. L., Corsini, E. M., & Simonneau, E. 2008, A&A, 478, 353
Muzzin, A., Marchesini, D., Stefanon, M., et al. 2013, ApJ, 777, 18
Naab, T., Johansson, P. H., & Ostriker, J. P. 2009, ApJL, 699, L178
Newman, A. B., Ellis, R. S., Andreon, S., et al. 2014, ApJ, 788, 51
Newman, A. B., Ellis, R. S., Bundy, K., & Treu, T. 2012, ApJ, 746, 162
Nipoti, C., Treu, T., Leauthaud, A., et al. 2012, MNRAS, 422, 1714
Oke, J. B., & Gunn, J. E. 1983, ApJ, 266, 713
Oser, L., Naab, T., Ostriker, J. P., & Johansson, P. H. 2012, ApJ, 744, 63
Peng, Y.-j., Lilly, S. J., Kovač, K., et al. 2010, ApJ, 721, 193
Poggianti, B. M., Calvi, R., Bindoni, D., et al. 2012, arXiv:1212.3207
Poggianti, B. M., Moretti, A., Calvi, R., et al. 2013, ApJ, 777, 125
Ragone-Figueroa, C., & Granato, G. L. 2011, MNRAS, 414, 3690
Rutkowski, M. J., Jeong, H., Cohen, S. H., et al. 2014, ApJ, 794, 101
Salimbeni, S., Fontana, A., Giallongo, E., et al. 2009, in AIP Conf. Ser. 1111, ed. G. Giobbi et al. (Melville, NY: AIP), 207
Salpeter, E. E. 1955, ApJ, 121, 161
Saracco, P., Longhetti, M., & Gargiulo, A. 2011, MNRAS, 412, 2707
Sérsic, J. L. 1963, BAAA, 6, 41
Shen, S., Mo, H. J., White, S. D. M., et al. 2003, MNRAS, 343, 978
Sonnenfeld, A., Nipoti, C., & Treu, T. 2014, ApJ, 786, 89
Thomas, D., Maraston, C., Bender, R., & Mendes de Oliveira, C. 2005, ApJ, 621, 673
Trujillo, I., Cenarro, A. J., de Lorenzo-Cáceres, A., et al. 2009, ApJL, 692, L118
Trujillo, I., Conselice, C. J., Bundy, K., et al. 2007, MNRAS, 382, 109
Trujillo, I., Ferreras, I., & de La Rosa, I. G. 2011, MNRAS, 415, 3903
Valentinuzzi, T., Poggianti, B. M., Saglia, R. P., et al. 2010, ApJL, 721, L19
van der Wel, A., Franx, M., van Dokkum, P. G., et al. 2014, ApJ, 788, 28
van der Wel, A., Rix, H.-W., Wuyts, S., et al. 2011, ApJ, 730, 38
van Dokkum, P. G., Bezanson, R., van der Wel, A., et al. 2014, ApJ, 791, 45
Whitaker, K. E., Kriek, M., van Dokkum, P. G., et al. 2012, ApJ, 745, 179